

First images of 6.7-GHz methanol masers in DR21(OH) and DR21(OH)N

L. Harvey-Smith^{1,2*}, R. Soria-Ruiz¹, A. Duarte-Cabral^{1,3,5} and R.J. Cohen^{4*†}

¹*Joint Institute for VLBI in Europe, Postbus 2, 7990 AA Dwingeloo, The Netherlands.*

²*School of Physics, University of Sydney, 2006 NSW, Australia.*

³*Departamento de Física da Faculdade de Ciências da Universidade do Porto, Rua do Campo Alegre 687, 4169 - 007 Porto, Portugal.*

⁴*University of Manchester, Jodrell Bank Observatory, Macclesfield, Cheshire, SK11 9DL, United Kingdom.*

⁵*Jodrell Bank Centre for Astrophysics, University of Manchester, Alan Turing Building Oxford Road, Manchester, M13 9PL, United Kingdom.*

26 November 2021

ABSTRACT

The first images of 6.7-GHz methanol masers in the massive star-forming regions DR21(OH) and DR21(OH)N are presented. By measuring the shapes, radial velocities and polarization properties of these masers it is possible to map out the structure, kinematics and magnetic fields in the molecular gas that surrounds newly-formed massive stars. The intrinsic angular resolution of the observations was 43 mas (~ 100 AU at the distance of DR21), but structures far smaller than this were revealed by employing a non-standard mapping technique. By plotting the positions of the Gaussian-fitted maser emission centroids in each velocity channel, the internal velocity gradients of the masers were investigated at very high spectral and spatial resolution. This technique was used in an attempt to identify the physical structure (e.g. disc, outflow, shock) associated with the methanol masers. Two distinct star-forming centres were identified. In DR21(OH) the masers had a linear morphology, and the individual maser spots each displayed an internal velocity gradient in the same direction as the large-scale structure. They were detected at the same position as the OH 1.7-GHz ground-state masers, close to the centre of an outflow traced by CO and class I methanol masers. The shape and velocity gradients of the masers suggests that they probably delineate a shock. In DR21(OH)N the methanol masers trace an arc with a double-peaked profile and a complex velocity gradient. This velocity gradient closely resembles that of a Keplerian disc. The masers in the arc are 4.5% linearly polarized, with a polarization angle that indicates that the magnetic field direction is roughly perpendicular to the large-scale magnetic field in the region (indicated by lower angular resolution measurements of the CO and dust polarization). The origin and nature of these maser structures is considered within the context of what is already known about the region. The suitability of channel-by-channel centroid mapping is discussed as an improved and viable means to maximise the information gained from the data.

Key words: masers – stars: formation – polarization – ISM: molecules – radio lines: ISM – ISM: individual DR21

1 INTRODUCTION

The DR21 star-forming complex is a large and highly active region, containing many sites of recent and ongoing star-formation as evidenced by observations of atomic and molecular gas and dust at a wide range of frequencies. It lies in the Cygnus X region of our Galaxy at a kinematical distance estimated to be between 2 and 3 kpc (Dickel & Wendker 1978; Campbell et al. 1982; Piepenbrink &

Wendker 1988; Odenwald & Schwartz 1993). DR21 contains many sub-regions denoted by positions of Infra-Red Sources (IRSs), Far Infra-Red sources (FIRs) or Extremely Reddened Objects (EROs), which are interpreted as sites of ongoing star-formation (e.g. Kumar et al. 2007; Jakob et al. 2007). This paper will describe the results of Multi-Element Radio-Linked Interferometer Network (MERLIN) observations of class-II methanol masers at 6.7-GHz in two regions of active massive star-formation within DR21.

The aim of this work is to understand the role of outflows, circumstellar discs and magnetic fields in the forma-

* E-mail: lhs@usyd.edu.au

† Deceased

tion of massive stars. This can be achieved by studying the 6.7-GHz methanol masers at high spatial and spectral resolution. It is possible to effectively enhance the resolving power of MERLIN by measuring the centroid positions of the maser emission in each spectral channel of the maser line. This, coupled with linear and/or circular polarization information on the masers allows us to form a 3-dimensional + magnetic field picture of the physical region immediately surrounding emerging massive stars.

This work is part of an on-going study of several regions of massive star-formation that produce bright OH and methanol masers. Data from phase-referenced observations at 1.7, 4.7, 6.0 and 6.7-GHz are also available to the authors. This sample covers all the OH and methanol maser lines that can be observed within the working frequency range of MERLIN. Parts of this survey have already been published (Harvey-Smith & Cohen 2005; Nammahachak et al. 2006; Green et al. 2007) but the mapping of several regions is on-going. Most of the observations in the multi-frequency study were correlated in full polarization mode, and it is therefore possible to measure the properties of magnetic fields in these regions, as well as the Faraday rotation (e.g. Vlemmings, Harvey-Smith & Cohen 2006). The goal of this survey is to map all the maser lines listed above in full polarizations, thus forming an in-depth picture of several regions of massive star-formation from which to draw specific conclusions about the relationship between masers, magnetic fields and stellar accretion.

2 OBSERVATIONS

The 5_1-6_0 A^+ 6668.518 MHz methanol emission from DR21(OH) (also known as W75S or W75S(OH)) and DR21(OH)N (also called W75) was observed between January 12th and 14th 2005 using five telescopes of MERLIN: the Mark II telescope at Jodrell Bank and the outstation telescopes at Cambridge, Darnhall, Knockin and Pickmere. The longest baseline was 218 km, giving a minimum fringe spacing of 43 mas at 6.7 GHz. A spectral bandwidth of 0.5 MHz was employed for the line observations (narrow-band mode) and this was split into 512 frequency channels. The data were correlated in full polarization mode. The radial velocity range was 22.5 km s^{-1} , centred on a velocity of 5 km s^{-1} . The velocity resolution was 0.0439 km s^{-1} . Here and elsewhere radial velocities are given relative to the local standard of rest. For observations of the phase-calibrator source 2005+403, a 16-MHz bandwidth was split into 16 channels (wide-band mode) and then averaged into a single channel. Every 6 or 7 minutes on DR21(OH) in narrow-band mode was followed by a 2 minute period on the phase-calibrator in the wide-band mode. The same procedure was followed for DR21(OH)N. At 6.7 GHz, the total time spent on each target source was 2 hours. In addition, two longer periods (a total of 4 hours) were spent on the bandpass calibrator source 3C84, switching between wide-band and narrow-band modes (after a 3 minute observation period in each mode). Another two extended periods of a total of 4 hours were spent on the primary flux and polarization-angle calibrator 3C286 (again switching from wide-band and narrow-band modes every 3 minutes).

Instrumental feed polarization was determined using

AIPS task PCAL. After determining the phase offset between the RCP and LCP signals, self-calibration was performed on a strong and compact maser feature using the left circular polarization image. The calibration results were then applied to both polarizations. A sample of 5 maser features were tested, but no statistically significant shift in the positions of the masers was found before and after self-calibration had been applied. The absolute polarization angle of the masers was determined using 3C286, which has a known polarization position angle of 33° .

A region of 512×512 pixels ($7''.68 \times 7''.68$) was imaged in Stokes I,Q,U and V with a pixel size of 15 mas. A circular restoring beam of 50 mas was used in the AIPS task IMAGR. In order to improve the signal-to-noise ratio of the images, self-calibration was applied to the Stokes-I image before the positions and velocities of the masers was calculated.

A careful search of the MERLIN 6.7 GHz Stokes-I image led to the identification of all the methanol maser flux in DR21(OH) and DR21(OH)N within the calibration errors. This was in the form of compact, but elongated, methanol masers. Two-dimensional Gaussian components were fitted to the images using the AIPS routine ORFIT and the positions and peak velocities of the maser components in each channel were found.

For this study, a maser was deemed to exist where an emission feature with a minimum flux density of 5 times the RMS noise level in that channel appeared in at least six adjacent velocity channels. It became clear however, that rather than being simple maser spots, the vast majority of maser components had significant internal structure, meaning that the automatic assignment of mean positions and velocities to maser spots would lead to a loss of information. The data are therefore presented both as maser spots and as Gaussian-fitted centroid positions of the maser emission in individual channels. As the following sections will show, this technique has led to much greater understanding of the masers, including their morphologies and radial velocity profiles.

3 RESULTS

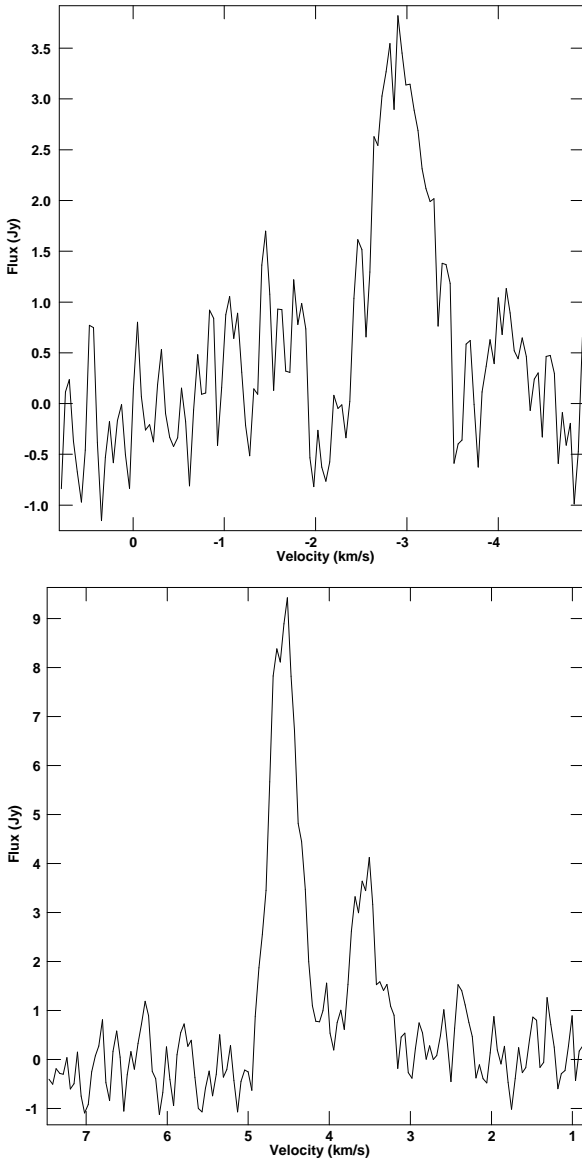
3.1 Overview of results

Two sites of 6.7-GHz methanol emission were detected within the DR21 star-forming complex. This was in the form of a group of five maser spots in DR21(OH) and three maser spots in DR21(OH)N. Two of the spots in DR21(OH)N seem to make up a single physical structure which is producing linearly polarized methanol masers. No existing maps of 6.7-GHz methanol maser emission in these regions have been found and so all the masers in this paper are thought to be new discoveries. Table 1 lists the flux weighted mean positions, peak flux densities, brightness temperatures, velocities and linewidths of the maser spots in DR21(OH)N and DR21(OH). Figure 1 shows the spectra measured at 6.7 GHz. There are clearly two strong maser peaks in DR21(OH)N, whereas DR21(OH) shows a single, weaker and more extended peak.

In the following sections, the properties of the masers found in each region are discussed in more detail.

Table 1. Parameters of 6.7-GHz methanol masers in DR21(OH) and DR21(OH)N.

Maser Spot Number	R.A. (J2000) ($20^h 39^m \text{ }^s$)	Dec. (J2000) ($42^\circ 24' \text{ }''$)	Peak Flux Density (Jy beam $^{-1}$)	Lower Limit to Peak T_b (K)	Velocity (km s $^{-1}$)	$\Delta V_{1/2}$ (km s $^{-1}$)
1	0.377	37.145	9.280	1.48×10^8	4.555	0.38
2	0.379	37.150	4.801	7.64×10^7	3.559	0.25
3	0.373	37.182	0.253	4.03×10^6	3.199	0.12
	($20^h 39^m \text{ }^s$)	($42^\circ 22' \text{ }''$)				
4	1.052	49.177	1.610	2.56×10^7	-2.800	0.28
5	1.074	49.287	0.303	4.82×10^6	-3.109	0.20
6	1.066	49.233	0.848	1.35×10^7	-3.133	0.20
7	1.071	49.257	0.450	7.16×10^6	-3.401	0.13
8	1.026	49.026	0.537	8.55×10^6	-3.887	0.25


Figure 1. Methanol 6.7-GHz maser spectra in DR21(OH) (top) and DR21(OH)N (bottom).

3.2 DR21(OH)

By plotting the positions of Gaussian-fitted centroids of the maser emission channel-by-channel, the velocity gradients within DR21(OH) were mapped out in great detail. Figure 2 shows the positions of the 6.7-GHz maser emission above $5\sigma_{RMS}$ in each spectral channel in DR21(OH). The elongation of the maser emission is clear, with all the maser spots sharing a common position angle in this region. It is interesting to note that each maser spot is elongated in the same plane as the large-scale structure. Each spot has an internal velocity gradient with the same orientation, although the region as a whole has no clear velocity gradient. This strongly indicates that the linear arrangement of methanol masers delineates neither a circumstellar disc nor an outflow. One explanation could be that the molecular cloud as a whole is rotating, and the masers are triggered by a shock propagating through the cloud. Thus the individual maser groups have very similar velocity gradients along their length. This model will be discussed further in Section 4.1.

Figure 3 (left) shows flux density contours of the 6.7-GHz maser emission in DR21(OH), integrated between 2.6 and 4.1 km s $^{-1}$. Figure 3 (right) shows the velocity versus R.A. through the maser structure, integrated over all declinations across the feature. This reveals that the linear structure is actually split into three separate sections, marked A, B, and C, each sharing a similar velocity gradient but having a separate location on the sky.

3.3 DR21(OH)N

Positions of the Gaussian-fitted centroids of the maser emission in DR21(OH)N are plotted channel-by-channel in Figure 4. There are three maser ‘spots’ by the common definition (as described in the Introduction), however there appear to be only two separate physical structures traced by maser emission, each of which has an ordered velocity gradient. These maser features will be referred to as components 1 and 2.

Component 1 has a fascinating arc structure, with velocities ranging from 3.2 to 4.9 km s $^{-1}$ at either end. This feature has an internal velocity gradient that is complex but very well sampled. Figure 5 shows this velocity gradient along the major (East–West) axis across the 39 spectral channels showing maser emission to a level of $5\sigma_{RMS}$ in this

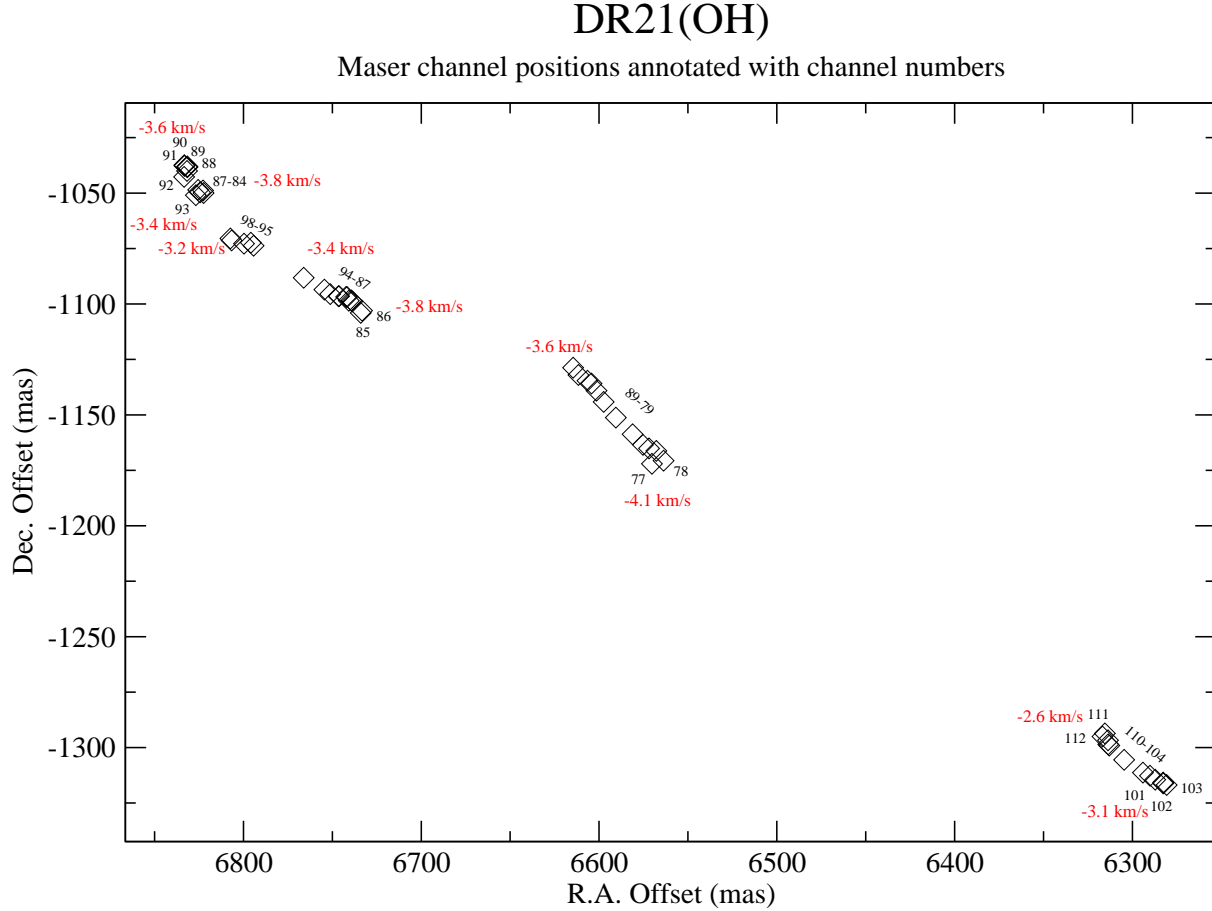


Figure 2. Channel-by-channel positions of 6.7-GHz methanol masers in DR21(OH), annotated with channel numbers. R.A. and Dec. offsets are relative to the map centre at $20^{\circ}39'00''.4570 +42^{\circ}22'50''.330$. The maser emission is clearly aligned along a linear structure, ~ 0.7 arcseconds in length. Within each group of masers indicated on the map (i.e. within each maser spot), the redshifted velocity increases systematically towards the West, directly along the linear structure. However, there is no global velocity gradient across the region as a whole.

feature. Its shape resembles the Keplerian rotation curve of an edge-on disc, however there are clearly some deviations from this behaviour. It has a linear velocity gradient through the central region near channels 84 and 85, where the radial velocity changes very little across the ~ 20 mas width of the feature. Then there are the two Keplerian-like portions of the structure.

Figure 6 shows the polarization properties of the masers in DR21(OH)N. There two large peaks in the spectrum of linear polarization; these occur in the West and East of the maser component 1. These maser spots are 4.9% and 4.5% linearly polarized respectively. Both peaks share a linear polarization angle of approximately -40° , although there appears to be a linear gradient in polarization angle, with the orientation changing by 20 degrees across the feature. Assuming that the magnetic field direction is perpendicular to the linear polarization vectors (Vlemmings et al. 2006), the mean orientation of the magnetic field vectors in DR21(OH)N is $+50^{\circ}$ East of North.

Component 2 is simple in morphology, unpolarized, and has a linear velocity gradient across the feature between 3.1

and 3.3 km s^{-1} . In the following sections, these results will be discussed in the context of what is already known about the regions.

4 DISCUSSION

4.1 The molecular environment of DR21(OH)

DR21(OH) appears to be composed of two deeply embedded star-forming cores, called MM1 and MM2, which are traced by 1.4 and 2.7 mm continuum emission from dust and $J = 2 \rightarrow 1$ C^{18}O (Woody et al. 1989, Padin et al. 1989, Magnum, Wooten & Mundy 1991, Lai, Girart & Crutcher 2003). The cores are young, having no visible HII region and therefore no continuum emission is seen from the region at centimeter wavelengths. From measurements of the far infra-red luminosity, MM1 is thought to contain a B0.5 V ZAMS star (Magnum, Wooten & Mundy, 1992). The MM1 core also contains ground-state OH masers at 1.6 GHz near the peak of the dust continuum emission (Norris et al. 1982; Fish et al. 2005). Next to MM1 is MM2, a dense and massive

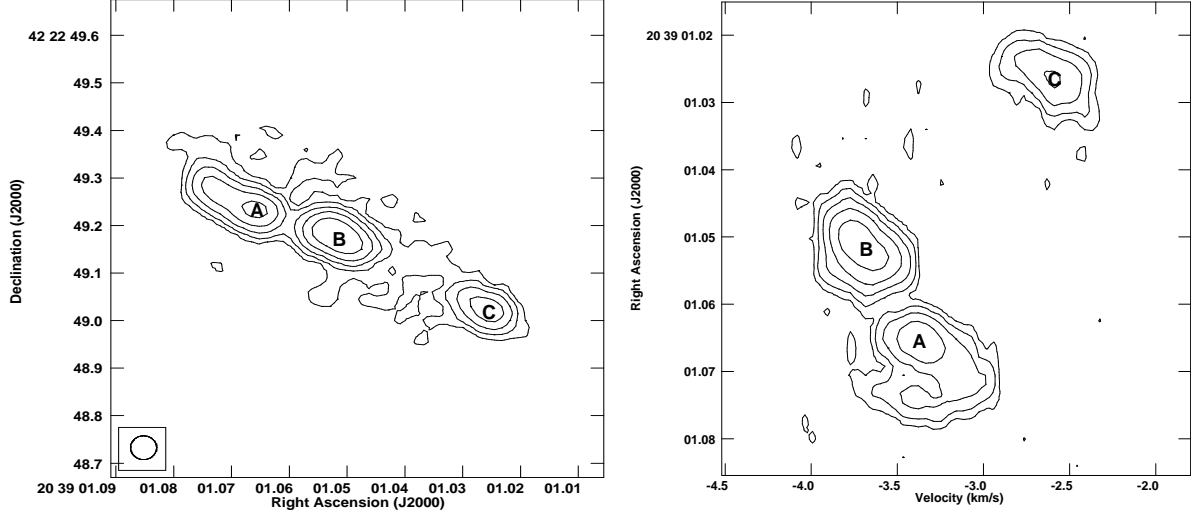


Figure 3. Left: Methanol 6.7-GHz maser flux in DR21(OH), integrated between 2.6 and 4.1 km s⁻¹. The peak flux is 186 mJy/beam and the contour levels are $6 \times (1, 2, 4, 8, 16, 32, 64, 128, 256, 512, 1024)$ mJy beam⁻¹. Right: Velocity–R.A. plot of the region. Sections A, B and C have similar velocity gradients, although section C is moving towards us with a greater velocity than sections A and B. The fact that the velocity gradient is similar in each section of the filament suggests that this is caused by a bulk rotation in the cloud.

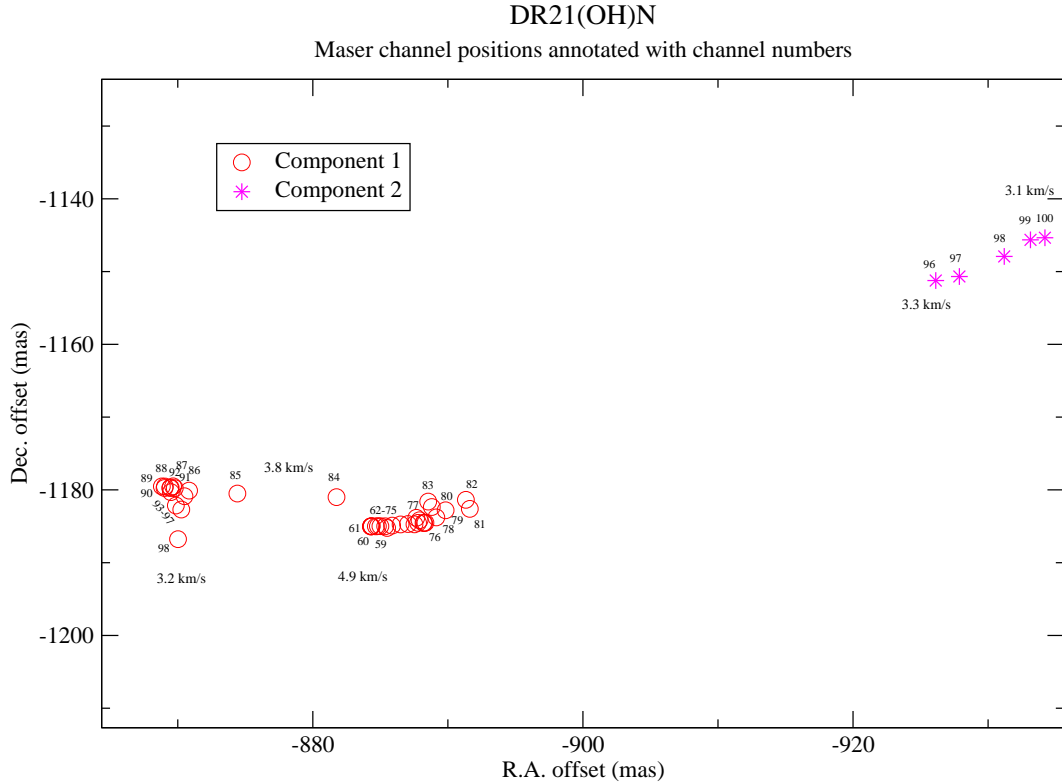


Figure 4. Map of 6.7-GHz methanol masers in DR21(OH)N. Symbols represent the Gaussian fitted centres of emission in each spectral channel with signal above 5σ times the RMS noise level in that channel. R.A. and Dec. offsets are relative to the map centre at $20^{\circ}39'00''.4570 + 42^{\circ}24'38''.330$. There are three separate maser spots, although two of these (spot numbers 1 and 2 in Table 1) appear to be physically associated. Here they are referred to collectively as component 1.

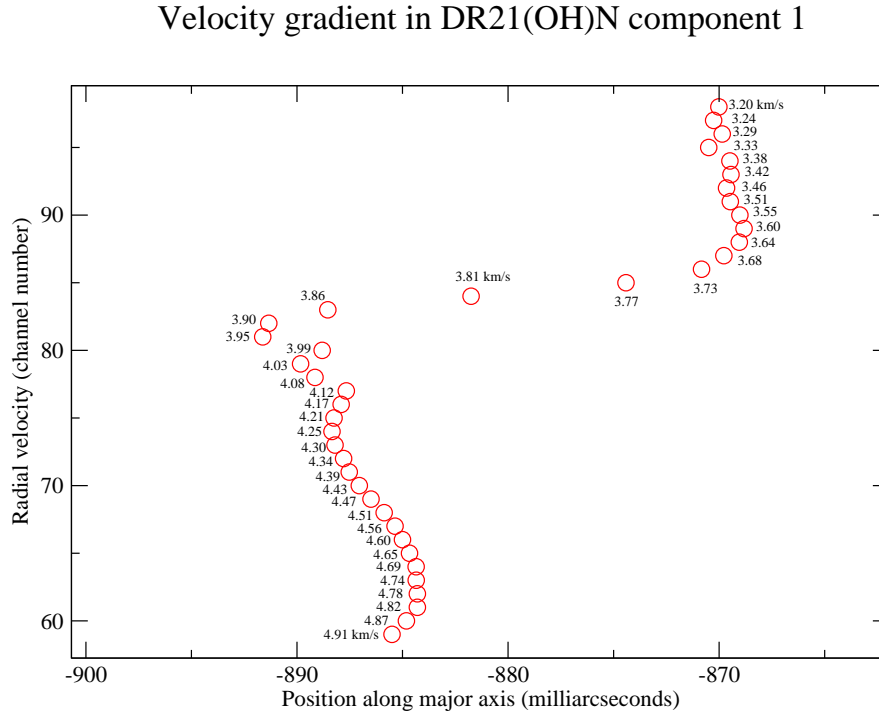


Figure 5. The velocity gradient of component 1 along its major (East–West) axis. Each symbol represents a single spectral channel and is labelled with the central velocity in km s^{-1} . The structure is well sampled, with 39 velocity channels having a signal greater than 5σ times the RMS noise level. The position along the major axis is measured in milliarcseconds, relative to the pointing centre of the image.

($480 M_{\odot}$) condensation which, according to estimates of the dust temperature, may contain at least one massive early-B type star (Magnum et al. 1991). Interferometric observations of NH_3 (1,1) emission using the VLA resolved MM2 into two components, called MM2–A and MM2–B (Magnum et al. 1992).

Centred approximately on the MM1 and MM2 cores, there is a region of extended methanol continuum emission which, towards its outer edges, contains class I methanol masers at 36 GHz (Haschick & Baan 1989), 44 GHz (Haschick, Menten & Baan 1990), 81 and 84 GHz (Batra & Menten 1988) and 95 GHz (Plambeck & Menten 1990). Measurements of the methanol continuum, CO $J = 3 - 2$ emission and the Class I methanol masers all suggest the presence of an outflow centred close to MM1/MM2 which is aligned approximately East–West (Lai et al. 2003; Vallee & Fiege 2006).

Perpendicular to this outflow is an extended region of CS molecular emission, mapped by Chandler et al. (1993), which is part of the large-scale molecular ridge in DR21. Water masers at 22 GHz have been observed to coincide with this CS line (Genzel & Downes 1977; Magnum et al. 1992). The morphology of water masers detected in DR21(OH) are not consistent with an outflow, rather they appear to have formed at the shock boundaries of expanding stellar shells centred on the star-forming cores MM1, MM2–A and MM2–B.

The magnetic field direction in DR21(OH) – as elsewhere in the DR21 complex – has been determined to be perpendicular to the large-scale North–South finger of gas and dust that connects the individual star-forming regions (Lai et al. 2003; Vallee & Fiege 2006). Unfortunately, the methanol maser emission in DR21(OH) was unpolarized and therefore no additional information can be added on the magnetic field.

4.2 A filament of methanol masers in DR21(OH)

A line of 6.7-GHz methanol masers was detected, that appears to be associated with the OH masers at the central peak of MM1. This 1.4mm continuum source is thought to house an embedded pre-main sequence B-type star. The maser filament in DR21(OH) is well sampled in position and velocity space (see Figure 2). By studying the velocity gradients channel-by-channel, it becomes clear that the maser spots each have independent but similar velocity gradients. There is no clear systematic velocity gradient for the whole region however, which precludes the possibility of this maser filament delineating a single disc or outflow. The linear maser spots appear not to be tracing individual circumstellar discs either, as the calculated masses of the central stars (assuming Keplerian rotation) are small fractions of a solar mass ($\sim 10^{-2} M_{\odot}$). Instead, the spatial morphology seems to indicate that the masers were most likely to

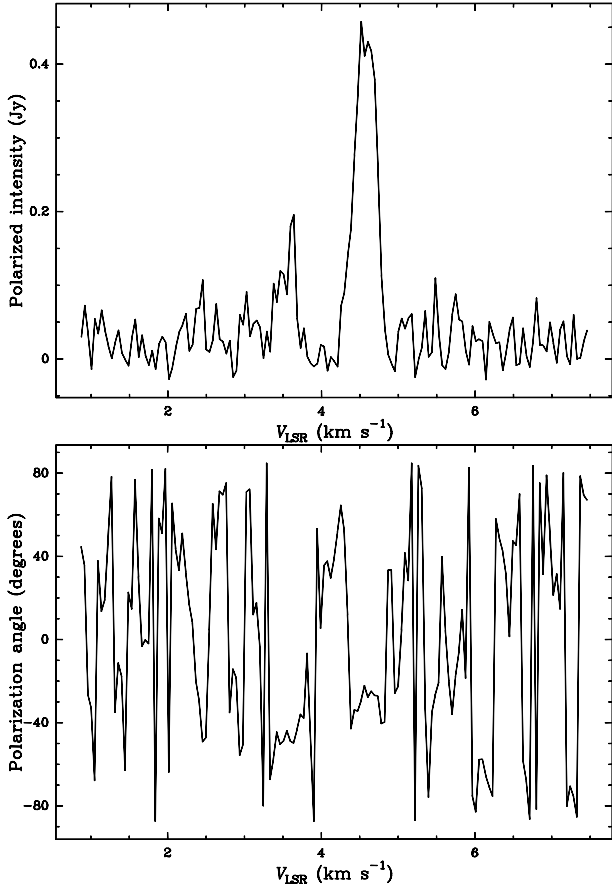


Figure 6. The polarization properties of DR21(OH)N. The linear polarization spectrum (top) shows a large and a smaller peak, which correspond to the West and East regions of component 1, respectively. The polarization angle plot (bottom) shows two coherent sections at the velocities of the peaks in polarized intensity, with a polarization position angle of around -40° . There appears to be a linear gradient in the polarization position angle across component 1.

have been formed in a shock passing through a turbulent or clumpy medium.

Dodson, Ojha & Ellingsen (2004) proposed a model to explain the high prevalence lines or arcs within methanol masers. They described a scheme in which the masers arise in planar shocks travelling perpendicular to the line-of-sight. Their model fitted with their observations of velocity gradients within individual methanol maser spots at 6.7 GHz that were perpendicular to the orientation of the lines or arcs of masers. In contrast, the opposite appears to be true in DR21(OH). Here, the internal velocity gradients of the masers are parallel to the direction of the linear extension. This could still be compatible with the passage of an edge-on shock if (1) the rotation velocity of the cloud as a whole were much greater than the velocity of the shock, in other words, there was a near-stationary density enhancement in the rotating star-forming cloud, or (2) the masers were produced in a very narrow region of the shock, so the motion of the shock itself is not visible in the velocity gradient of the maser.

4.3 DR21(OH)N – methanol masers in a protostellar disc?

The 6.7-GHz methanol maser emission found near DR21(OH)N coincides with the bright $8\ \mu\text{m}$ source ERO3 within the 0.4 arcsecond positional uncertainties of the *Spitzer* IRAC survey (Marston et al. 2004; Davis et al. 2007). ERO3 has a spectral index (corrected for dust extinction) of 1.8 and it is thought to be a very young massive protostar that has not yet developed an HII region. It is therefore possible that component 1 represents a disc around the ERO3 protostar. The size of the disc traced by the methanol masers, assuming that the disc is seen edge-on and the masers are in a circular orbit, is approximately 60 AU. The velocity profile of the masers resembles the rotation curves (from observations and models) of the black hole disc in the nucleus of Centaurus A (Marconi et al. 2001). It is likely that the departure from a standard Keplerian rotation curve observed in DR21(OH)N is caused by a combination of factors; namely an inclination of the disc to our line-of-sight and a difference between our selected East–West disc major axis and the true orientation. Existing MERLIN OH maser data are currently being analysed to test whether the feature is seen in OH and to confirm the direction (and possibly the strength) of the magnetic field in DR21(OH)N. A proposal has been accepted by the European VLBI Network to observe the DR21 region at 6.7-GHz in order to independently measure the positions and velocities of this disc-like feature at milliarcsecond resolution. Lastly, a quantitative rotational model is being developed in order to determine the nature of this very interesting and unusual maser feature (Harvey-Smith et al. *in prep.*).

4.4 Magnetic fields in DR21

DR21(OH) is part of the much larger DR21 star-forming complex which is crossed by a prominent North–South finger of dust, seen in thermal $850\text{-}\mu\text{m}$ (e.g. Davis et al. 2007; Vallee & Fiege 2006) and 1.3 mm continuum emission (Lai et al. 2003). Comparisons of the CO and dust polarization characteristics by Lai et al. (2003) show that the magnetic field runs in roughly an E–W direction, perpendicular to the large-scale molecular ridge. Curran et al. (2005) also confirmed this magnetic field orientation by measuring dust and CO polarization in DR21(OH). Whilst the angular resolution of these studies was far lower than the MERLIN observations reported here, it is nevertheless possible to undertake a comparison of the magnetic field properties inferred from both the CO and dust emission (at $\sim 10''$ scales) and the methanol masers (at sub-arcsecond scales). The aims of such a comparison are (i) to facilitate an understanding of the variations in magnetic fields inside giant molecular clouds and (ii) to gauge the importance of magnetic fields in the process of protostellar accretion.

There is very little published information on the magnetic field in the vicinity of our linearly polarized methanol masers in DR21(OH)N. The only polarimetric data available is in the paper of Vallee & Fiege (2006). They measured the dust polarization at $850\text{-}\mu\text{m}$ using the James Clerk Maxwell Telescope and found, as in previous studies of DR21(OH)S and DR21(OH), that the inferred magnetic field direction is generally perpendicular to the North–South dust filament.

Their polarimetric data had an angular resolution of $14''$ and they binned squares of 3×3 pixels together, giving images with a pixel spacing of $9''$. In contrast, the MERLIN images of methanol masers from this paper have an intrinsic angular resolution of 50 mas and a pixel size of 15 mas. The dust polarization measurement closest in the sky to our polarized methanol masers gave a position angle of $172^\circ \pm 13^\circ$. This is not at all consistent with the methanol maser polarization position angle of 50° , which was measured at both the East and West points of methanol maser component 1.

So why does the magnetic field direction derived from observations of methanol masers disagree with previous measurements of CO and dust polarization by Vallee & Fiege (2006)? There is more than one possible explanation for this discrepancy. Firstly, the interpretation of the magnetic field direction from the measurements of CO or maser polarization angle may be incorrect. Goldreich, Keeley & Kwan (1973) showed quantitatively that, in the case that there is no circular polarization, the linear polarization produced by a maser is aligned either parallel or perpendicular to the projection of the magnetic field on the plane orthogonal to the direction of propagation of the maser. The polarization of CO suffers a similar ambiguity in magnetic field direction (Goldreich & Kylafis 1982), so it is possible that the magnetic field direction is in fact parallel to the large-scale dust lane in DR21. Such a mis-interpretation is very unlikely because, in polarization studies of CO, simultaneous observations of dust polarization have always been used to unwrap this ambiguity (e.g. Lai et al 2003; Vallee & Fiege 2006).

Secondly, the polarization of our methanol maser component 1 may have been caused by a *local* magnetic field (e.g. close to a massive protostar) and this field would be different to the larger-scale magnetic field across the gas and dust lane. This view is supported by observations of OH polarization in DR21(OH) by Fish et al. (2005), who found large variations in the direction of the local magnetic field inferred from the polarization of OH ground-state masers in MM1, although it is possible that these apparent variations are caused by Faraday rotation and not small-scale changes in the magnetic field (Fish & Reid 2006). If masers show larger variations in linear polarization angle within a region than the dust or CO polarization angles, this suggests that masers (as high-resolution tracers) delineate very localised magnetic field structure. This is clearly very helpful in our attempt to understand the contribution of magnetic fields to individual sites of massive star-formation. The next step is to determine the polarization properties of OH masers at 1.7-GHz and 6.0-GHz from existing MERLIN data (taking into account differential Faraday rotation), thus providing independent measurements of the magnetic field direction on ~ 1000 AU (individual maser) scales. Another independent test of the magnetic field in this region will be high-resolution polarimetric dust and CO observations. The magnetic fields inferred from dust and CO polarization are much smoother than those inferred by maser observations, but this may well be an artefact of the much larger beamsizes of the instruments. Dust and/or CO polarization observations at comparable angular resolution to MERLIN should be carried out before conclusions are drawn about the small-scale magnetic fields in the region.

4.5 Interior structure of maser spots

By mapping the positions of the Gaussian-fitted 6.7-GHz methanol maser centroids in each velocity channel, we have probed the interior structure of individual maser components in regions significantly smaller than the (50×50 mas) MERLIN beam. High spectral-resolution studies such as these have previously been carried out using the VLBA at 12.2 GHz by Moscadelli et al. (2003) and at 18-cm by Fish et al. (2006). Despite the much larger beam of the MERLIN observations, our results are remarkably similar to those from the VLBA, in that we have been able to map structures such as lines and arcs within regions smaller than 20 mas. The shape and velocity profile of the structure found with MERLIN must be verified using VLBI, but it is interesting to note that by fitting Gaussians to individual spectral channels, an ‘effective angular resolution’ (the ability to distinguish the movement of the central peak flux position) an order of magnitude greater than the true angular resolution of MERLIN has been achieved. Follow-up observations have now been made with the European VLBI Network, which will form the basis of a future paper by Harvey-Smith & Soria-Ruiz.

5 CONCLUSIONS

By observing the DR21 star-forming complex at 6.7-GHz, two new sites of methanol maser emission in DR21(OH) and DR21(OH)N have been found. Two dimensional Gaussian components were fit to the emission in each spectral channel containing a signal greater than $5\sigma_{RMS}$. The positions of the emission centroids in each channel were then mapped, in an attempt to determine the internal velocity gradients of the maser spots. This technique added a great deal of information about the structures traced by the methanol masers, which is vital to our aim of linking methanol masers to physical features such as discs around protostars and outflows of circumstellar material. The maser feature in DR21(OH)N, component 1, is a strong candidate to be a circumstellar disc. It has a double-peaked spectral profile, a complex velocity gradient that resembles a Keplerian rotation curve and a magnetic field gradient across its major axis. It also coincides with a massive protostar that has been previously identified by studies of infra-red and dust emission. Further study of the existing MERLIN 1.7-GHz and 6.0-GHz OH maser data in full polarizations and high-resolution European VLBI Network data of methanol at 6.7-GHz will hopefully add to our understanding of the disc-like component 1 in particular. Numerical analysis of the feature in terms of a Keplerian rotation model will reveal whether or not this feature is likely to be a disc around a massive protostar.

ACKNOWLEDGMENTS

The authors thank the referee, Thomas Wilson, for his useful comments. Lisa Harvey-Smith thanks Vincent Fish for very helpful discussions regarding the AIPS task ORFIT. Ana Duarte-Cabral acknowledges the support of a JIVE Summer Studentship. MERLIN is a National Facility operated by the University of Manchester at Jodrell Bank Observatory on behalf of STFC.

REFERENCES

- Baars J.W.M., Genzel R., Pauliny-Toth I.I.K., Witzel A., 1977, *A&A*, 61, 99.
- Batrla W., Menten K.M., 1988, *ApJ*, 329, 117.
- Campbell M.F., Niles D., Nawfel R., Hawrylycz M., Hoffmann W.F., Thronson, H.A., Jr., 1982, *ApJ*, 261, 550.
- Chandler C.J., Moore T.J.T., Mountain C.M., Yamashita T., 1993, *MNRAS*, 261, 694.
- Curran R. L., Collett J. L., Atkinson J. W., Chrysostomou A., Aitken D. K., 2005, in *Protostars and Planets V*, Proceedings of the Conference held October 24-28, 2005, in Hilton Waikoloa Village, Hawai'i. LPI Contribution No. 1286., p.8160.
- Davis C.J., Kumar M.S.N., Sandell G., Froebrich D., Smith M.D., Currie M.J., 2007, *MNRAS*, 374, 29.
- Dickel H. R., Wendker H. J., 1978, *A&A*, 66, 289.
- Dodson R., Ojha R., Ellingsen S. P., 2004, *MNRAS*, 351, 779.
- Fish V. L., Reid M. J., Argon A. L., Zheng X-W., 2005, *ApJSS*, 160, 220.
- Fish V. L., Reid M. J., 2006, *ApJSS*, 164, 99.
- Fish V. L., Bricken W.F., Sjouwerman L.O., 2006, *ApJ*, 647, 418.
- Genzel R., Downes D., 1977, *A&AS*, 30, 145.
- Goldreich P., Keeley D.A., Kwan J.Y., 1973, *ApJ*, 179, 111.
- Goldreich P., Kylafis N.D., 1982, *ApJ*, 253, 606.
- Green, J.A., Richards, A.M.S., Vlemmings, W.H.T., Diamond P., Cohen R.J., *MNRAS* in press.
- Harvey-Smith L., Cohen R.J., 2005, *MNRAS*, 356, 637.
- Haschick A.D., Baan W.A., 1989, *ApJ*, 339, 949.
- Haschick A.D., Menten K.M., Baan W.A., 1990, *ApJ*, 354, 556.
- Jackob H., Kramer C., Simon R. Schnieder N., Ossenkopf V., Bontemps S., Graf U.U., Stutzki J., 2007, *A&A*, 461, 999.
- Kumar M.S.N., Davis C.J., Grave J.M.C., Ferreira B., Froebrich D., 2007, *MNRAS*, 374, 54.
- Lai S-P., Girart J.M., Crutcher R.M., 2003, *ApJ*, 598, 392.
- Marconi A., Capetti A., Axon D.J., Koekemoer A., Macchetto D., Schreier E.J., 2001, *ApJ*, 549, 915.
- Magnum J.G., Wootten A., Mundy L.G., 1991, *ApJ*, 378, 576.
- Magnum J.G., Wootten A., Mundy L.G., 1992, *ApJ*, 388, 467.
- Marston A.P. et al. 2004, *ApJSS*, 154, 333.
- Moscadelli L., Menten K. M., Walmsley C. M., Reid M. J., 2003, *ApJ*, 583, 776.
- Nammahachak S., Asanok K., Hutawarakorn Kramer B., Cohen R.J., Muanwong O., Gasipron N., 2006, *MNRAS*, 371, 619.
- Norris R. P., Booth R. S., Diamond P. J., Porter N. D., 1982, *MNRAS*, 291, 101.
- Odenwald S.F., Schwartz P.R., 1993, *ApJ*, 405, 706.
- Padin S., Sargent A. I., Mundy L. G., Scoville N. Z., Woody D. P., Leighton R. B., Masson C. R., Scott S. L., Seling T. V., Stapelfeldt K. R., Terebey S., 1989, *ApJ*, 337, L45.
- Piepenbrink A., Wednker H.J., 1988, *A&A*, 191, 313.
- Vallee J.P., Fiege J.D., 2006, *ApJ*, 636, 332.
- Vlemmings W.H.T., Harvey-Smith L., Cohen R.J., 2006, *MNRAS*, 371, L26.
- Plambeck R.L., Menten K.M., 1990, *ApJ*, 364, 555.
- Woody D.P., Scott S.L., Scoville N.Z., Mundy L.G., Sargent A.I., Padin S., Tinney C.G., Wilson C., 1989, *ApJ*, 337, L41.